ACS APPLIED MATERIALS & INTERFACES

Research Article

www.acsami.org

Role of the Interfaces in Multiple Networked One-Dimensional Core–Shell Nanostructured Gas Sensors

Sunghoon Park, Hyunsung Ko, Soohyun Kim, and Chongmu Lee*

Department of Materials Science and Engineering, Inha University, 253 Yonghyun-dong, Nam-gu, Incheon 402-751, Republic of Korea

Supporting Information

ABSTRACT: This study examined the gas sensing mechanism of multiple networked core–shell nanowire sensors. The ethanol gas sensing properties of In_2O_3/ZnO core–shell nanowires synthesized by the thermal evaporation of indium powder in an oxidizing atmosphere followed by the atomic layer deposition of ZnO were examined as an example. The pristine In_2O_3 nanowires and In_2O_3-core/ZnO-shell nanowires exhibited responses of ~30% and ~196%, respectively, to 1000 ppm ethanol at 300 °C. The response of the core–shell nanostructures to ethanol also showed a strong dependence on the shell layer width. The strongest response to ethanol was obtained with a shell layer thickness of ~44 nm corresponding to $2\lambda_D$, where λ_D is the Debye length of ZnO. The enhanced sensing properties of the core–shell nanowires toward ethanol can be explained based on the potential barrier-controlled carrier transport model combined with the surface depletion model; the former is predominant over the latter.

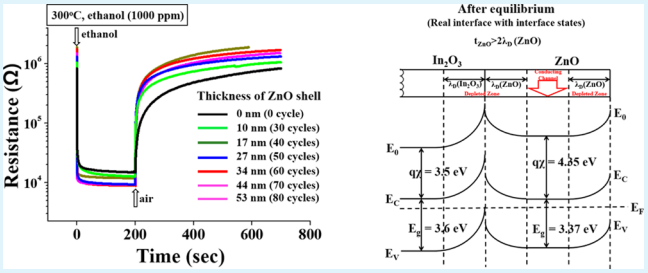

KEYWORDS: *In_2O_3 nanowires, core–shell nanostructures, gas sensors, ethanol, interfaces*

1. INTRODUCTION

In recent years, one-dimensional (1D) nanostructure-based sensors have become the focus of intensive research because of the advantages of higher sensitivity, superior spatial resolution, and rapid response associated with individual 1D nanostructures due to the high surface-to-volume ratios compared to thin film gas sensors.[1−3] On the other hand, enhancing their sensing performance and detection limit is still a challenge. The formation of core–shell nanostructures is one of the techniques developed to solve this problem. The enhanced gas sensing performances of many core–shell nanostructures have been reported.[4−14]

Regarding the sensing mechanism of core–shell 1D nanostructures, recently, Singh et al. reported that electron depletion layers form at the In_2O_3–ZnO interface because of the differences in work function of the core and shell materials as well as at the surface of ZnO shell in the In_2O_3–ZnO core–shell nanowires.[11] They emphasized the crucial role of the thicknesses of the depletion layers in carrier transport between sensing gas and nanowire material but did not report the optimal thickness. According to their report, along with the depletion layers, energy barriers at the internanowire contacts (homojunctions) and those at the potential barriers at core–shell interfaces (heterojunctions) have a profound effect on the final response of the sensor device. Katoch et al. reported the enhanced response of core–shell 1D nanostructures to CO gas compared to that of pristine 1D nanostructures.[15] They reported that the core–shell nanostructures showed the strongest response for the shell layer being equal to the Debye length λ_D of the shell material. Nevertheless, there is some controversy regarding the dependence of the sensing properties of core–shell nanostructures on the type of gas to be detected, the origin of the enhanced gas sensing properties, and the optimum shell layer thickness of core–shell nanostructures.

In_2O_3 is a typical n-type semiconductor with a wide direct bandgap of 3.55–3.75 eV. Over the past 2 decades, 1D In_2O_3 nanostructures[16−22] have been synthesized using a range of techniques and their gas-sensing properties have been widely explored. Many studies reported the excellent sensing properties of In_2O_3 toward a variety of gases such as O_3,[16,17] NO_2,[18,19] CO,[20] H_2.[21] On the other hand, the response of pristine In_2O_3 sensors to ethanol (C_2H_5OH) was not strong. The response of pure In_2O_3 nanowire sensors to 100 ppm of C_2H_5OH was less than 300%.[22] According to the literature, In_2O_3 nanowire sensors showed selectivity to C_2H_5OH gas over CH_4, CH_3OH, CH_3COCH_3, $(C_2H_5)_3N$ gases at 370 °C.[23] Furthermore, the sensors were quite insensitive to CO and H_2.[24]

This study examined the ethanol gas sensing properties of In_2O_3-core/ZnO-shell nanowires. The dependence of the ethanol gas sensitivity of the core–shell nanowires on the ZnO shell layer thickness was also analyzed. The sensing mechanism of the core–shell nanowires toward ethanol is discussed. In particular, the critical role of the potential barrier at the core–shell interface is emphasized. This paper also

Received: April 1, 2014
Accepted: May 21, 2014
Published: May 21, 2014

   dx.doi.org/10.1021/am501975v | ACS Appl. Mater. Interfaces 2014, 6, 9595–9600

discusses the origin of the enhanced sensing performances of several core−shell 1D nanostructures toward oxidizing gases.

2. EXPERIMENTAL SECTION

In_2O_3-core/ZnO-shell nanowires were prepared by thermal evaporation of In powders in an oxidizing atmosphere followed by the atomic layer deposition (ALD) of ZnO. First, Au-coated c-plane sapphire ((0001) Al_2O_3) substrates were used for the synthesis of one-dimensional (1D) In_2O_3 nanostructures. A 3 nm thick Au thin film was deposited on (0001) Al_2O_3 substrates by direct current (dc) magnetron sputtering. A quartz tube was mounted horizontally inside a tube furnace. 99.99% pure indium powder was placed on the lower holder at the center of the quartz tube. An Au-coated Al_2O_3 substrate was placed on the upper holder, approximately 5 mm away from the indium powder. The furnace was heated to 800 °C and maintained at that temperature for 1 h in a N_2/O_2 atmosphere with constant N_2 and O_2 flow rates of 100 standard cubic centimeter per minute (sccm) and 0.1 sccm, respectively. The total pressure was set to 1.0 Torr. Subsequently, ZnO thin films were deposited on the collected In_2O_3 by ALD. Diethylzinc (DEZn) and H_2O were fed alternately as source gases into the chamber separately. Typical feeding times for H_2O and DEZ were 0.15 and 0.2 s, respectively, and a typical purging time for the reactants was 3 s. The pressure and substrate temperature for a number of ALD process cycles in the chamber were 0.1 Torr and 150 °C, respectively. The ZnO shell layer thickness was controlled by the number of ALD process cycles. The number of ALD cycles used for forming ~27 nm thick ZnO shell layer was 50 cycles.

Scanning electron microscopy (SEM, Hitachi S-4200, 10 kV) and transmission electron microscopy (TEM, JEOL 2100F, 300 kV) were performed to examine the morphology and structure of the products. All SEM samples were prepared by placing small droplets of the solutions on silicon substrates and allowing the solvent to evaporate slowly by heating them at 40 °C for 24 h. The samples were then coated with 10 nm Pt thin film by dc sputtering. The TEM samples were prepared by placing a small droplet (~10 μL) of diluted reaction solutions 20 times on copper grids coated with amorphous carbon and then heating the solvent at 40 °C for 24 h. The crystal structure of the nanowires was determined by glancing angle X-ray diffraction (XRD, Philips X'pert MRD diffractometer) using Cu Kα radiation (λ = 0.1541 nm). For the gas sensing test two different types of multiple networked nanowire sensors, pristine In_2O_3 nanowire and In_2O_3-core/ZnO-shell nanowire sensors, were prepared. Each nanowire sample was dispersed ultrasonically in a mixture of deionized water (5 ml) and isopropyl alcohol (5 ml). The as-grown nanowires were placed onto the 200 nm thick SiO_2-coated Si(100) substrates equipped with a pair of interdigitated (IDE) Ni (~200 nm)/Au (~50 nm) electrodes with a gap of 20 μm. The flow-through technique was used to test the gas sensing properties. All the measurements were performed in a temperature-stabilized sealed chamber with a constant flow rate of 200 cm^3/min at 300 °C under 50% RH. The ethanol concentration was controlled by mixing ethanol gas with synthetic air with different ratios. The number of tested samples for each sensing test condition was three, and the response was determined by taking the average of the response values for those three samples.

The intersample reproducibility for the responses was quite high. Detailed procedures for sensor fabrication and sensing test have been presented elsewhere.[13] The sensor response to target gas is defined as $(R_a/R_g) \times 100$ (%), where R_a and R_g are the electrical resistances in the sensors in air and target gas, respectively.

3. RESULTS AND DISCUSSION

Figure 1a shows In_2O_3-core/ZnO-shell nanowires with a mean diameter of ~150 nm and lengths ranging from 10 to 30 μm. Figure 1b presents the XRD pattern of In_2O_3-core/ZnO-shell nanowires. Most peaks in the XRD pattern were assigned to the body-centered cubic-structured In_2O_3 with lattice constants of a = 1.011 nm (JCPDS no. 89-4595). In addition, several reflections from the (100), (002), and (101) lattice planes of

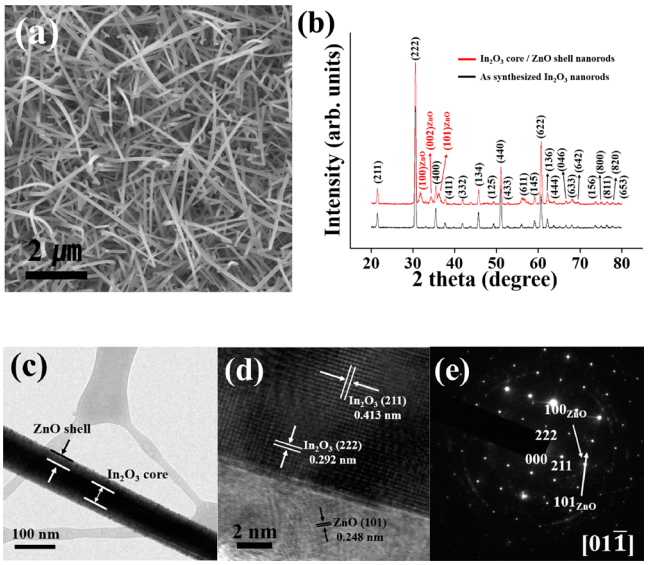

Figure 1. (a) SEM image of In_2O_3-core/ZnO-shell nanowires. (b) XRD patterns of In_2O_3-core/ZnO-shell nanowires. (c) Low-magnification TEM image of a typical In_2O_3-core/ZnO-shell nanowires. (d) High-magnification TEM image and (e) corresponding SAED pattern of the In_2O_3-core/ZnO-shell nanowires.

wurtzite-structured ZnO with lattice constants of a = 0.3253 nm, c = 0.5213 nm (JCPDS no. 89-1397) were identified, suggesting that the ZnO nanoparticles were also crystalline.

The low-magnification TEM image (Figure 1c) showed a typical In_2O_3-core/ZnO-shell nanowire with a rodlike morphology. High-resolution TEM (Figure 1d) revealed the In_2O_3−ZnO interface region in a typical In_2O_3-core/ZnO-shell nanowire, showing fringe patterns in both the In_2O_3 core and ZnO shell. The spacings of 0.413 and 0.292 nm in the fringe patterns were assigned to the interplanar distances of the {211} and {222} lattice planes in bulk crystalline In_2O_3, respectively, whereas the spacing of 0.248 nm corresponds to the interplanar distance of the {101} lattice plane in bulk crystalline ZnO. A dim concentric ring pattern and a spotty pattern with many clear spots were observed in the corresponding selected area electron diffraction pattern (Figure 1c). The bright spots were assigned to In_2O_3, while the dim concentric ring pattern was assigned to ZnO, suggesting that the In_2O_3 core was a single crystal and the ZnO shell was polycrystalline. Only one or two dim circles with relatively bright spots were observed in the ring pattern, suggesting that the number of grains in a ZnO shell was small; i.e., the mean grain size of the ZnO shell layers is relatively large compared to the shell layer thickness.

Figure 2a and Figure 2b show the sensor responses of the pristine In_2O_3 nanowires and In_2O_3-core/ZnO-shell nanowires, respectively, to ethanol pulses with concentrations of 200, 400, 600, 800, and 1000 ppm at 300 °C. The limit of detection of ethanol gas was ±2%. The resistance decreased reversibly upon each ethanol pulse. The electrical behavior of the sensors was consistent, recovering their original resistances without hysteresis after repeated exposure to ethanol gas at different concentrations. The pristine In_2O_3 nanowires showed responses of approximately 7.5−30.0% to 200−1000 ppm ethanol (Table 1). In contrast, the In_2O_3-core/ZnO-shell nanowires showed responses of approximately 18.8−196.2% to 200−1000 ppm ethanol (Table 1). The response to 1000 ppm ethanol gas was increased more than 6-fold by ZnO

dx.doi.org/10.1021/am501975v | ACS Appl. Mater. Interfaces 2014, 6, 9595−9600

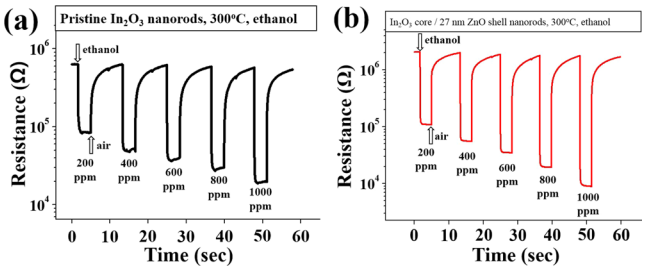

Figure 2. Electrical responses of the gas sensors fabricated from (a) pristine In2O3. (b) In2O3-core/ZnO-shell nanowires.

Table 1. Responses of Pristine In_2O_3 Nanowires and In_2O_3-Core/ZnO-Shell (27 nm) Banowires to 200−1000 ppm of C_2H_5OH Gas

	response, R_a/R_g (%)	
C_2H_5OH concn (ppm)	pristine In_2O_3	In_2O_3-core/ZnO-shell (27 nm)
200	7.47 ± 2.0	18.80 ± 2.0
400	13.15 ± 2.0	36.73 ± 2.0
600	17.52 ± 2.0	58.77 ± 2.0
800	22.10 ± 2.0	106.38 ± 2.0
1000	29.98 ± 2.0	196.15 ± 2.0

encapsulation. The response of the nanowire sensors to ethanol gas would be improved by increasing the sensing temperature.

Figure 3a and Figure 3b show the electrical responses of the In_2O_3-core/ZnO-shell nanowires with different shell layer

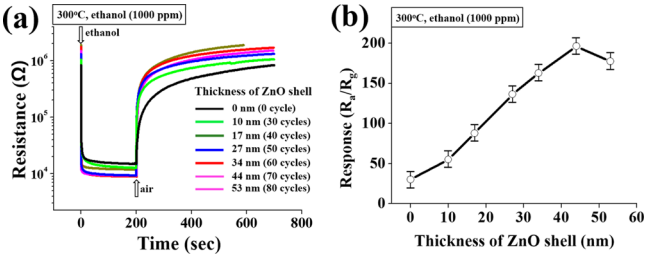

Figure 3. (a) Electrical responses of In_2O_3-core/ZnO-shell nanowires with different shell layer thickness to 1000 ppm ethanol gas at 300 °C. The number in parentheses is the number of ALD cycles for the corresponding ZnO shell layer thickness. (b) Response of In_2O_3-core/ZnO-shell nanowires to 1000 ppm ethanol gas as function of the shell layer thickness.

thicknesses to 1000 ppm ethanol gas and the plot of the response versus the ZnO shell layer thickness, respectively. The plot indicates that the response depends on the shell layer thickness strongly, implying that the sensing property of the core−shell nanowire sensor is intimately related to the depletion layer width. The strongest response was notably obtained for the shell layer thickness of 44 nm, which is very close to $2\lambda_D$(ZnO), where λ_D(ZnO) ≈ 21.7 nm.[13,15] This result suggests that the highest sensitivity is obtained for the ZnO shell layer thickness, $t_{ZnO} = 2\lambda_D$(ZnO), namely, for a maximum thickness of the ZnO shell layer completely depleted of electrons.

The ethanol gas sensing mechanism of the nanowire sensors can be explained using the surface-depletion model.[25] When the In_2O_3 nanowire sensor is exposed to air, it interacts with oxygen by transferring electrons from the conduction band of In_2O_3 to the adsorbed oxygen atoms, forming ionic species, such as O^-, O^{2-}, and O_2^- depending on the temperature.[26] The potential barrier increases as the number of oxygen ions on the surface increases, leading to higher resistance.[27] When the sensors are exposed to a reducing gas ethanol, ethanol molecules react with oxygen ions to form CO_2 and H_2O and generate electrons according to the following reactions. The electrons are released back into the nanowires:[28]

$$C_2H_5OH\,(gas) \rightarrow C_2H_5OH\,(ads) \quad (1)$$

$$C_2H_5OH\,(ads) + 6O^-\,(ads) \rightarrow 2CO_2\,(gas) + 3H_2O\,(gas) + 6e^- \quad (2)$$

This results in an increase in the carrier concentration of the sample and a decrease in depletion width. In other words, the depleted electrons are released back to the conduction band, decreasing the resistance of the sensors. Such adsorbed oxygen and large surface-to-volume ratio of the In_2O_3 nanowires increase the response of the nanowire gas sensors.

Figure 4a and Figure 4b show the energy band diagrams near the In_2O_3−ZnO heterojunction before and after equilibrium.[29−32] The electron affinities of In_2O_3 and ZnO are 3.5 [29] and 4.35 eV,[30] respectively, and the energy bandgaps of In_2O_3 and ZnO are 3.6 [31] and 3.37 eV,[32] respectively. The Debye lengths of In_2O_3 and ZnO are ∼25 [33] and 21.7 nm,[13,15] respectively. The precise Fermi energy levels (E_F) of undoped In_2O_3 and ZnO are not known, but it was assumed, considering their electron affinities and bandgap energies, that the E_F of In_2O_3 is somewhat higher than that of ZnO. Both undoped In_2O_3 and ZnO are n-type semiconductors. If n-type In_2O_3 and n-type ZnO are in contact with each other, electrons would transfer from In_2O_3 to ZnO until the Fermi energy levels (E_F) of the two materials become equal because the conduction band minimum (E_c) of In_2O_3 is higher than that of ZnO. Assuming that the In_2O_3−ZnO interface contains no interface states like the p-Si/n-Si junction or n^+-Si/n^--Si junction, the energy band of In_2O_3 would be bent upward, whereas that of ZnO would be bent downward near the In_2O_3−ZnO interface as shown in Figure 4b. Nevertheless, the actual In_2O_3−ZnO interface does have an interfacial layer or intermediate region sandwiched between the two materials and this interfacial layer contains a high density of surface states or interface states[34] like the outer surface of ZnO shell layer or the grain boundaries of polycrystalline materials because there is no coherency in atomic arrangement between In_2O_3 and ZnO becaue of lattice mismatch. Another phenomenon occurring in the two materials contacting with each other is trapping of the electrons, residing in both the In_2O_3 and ZnO near their interface, by the (acceptor-type) surface states in the interfacial layer. Overall, upon the formation of an In_2O_3−ZnO interface, the following two phenomena would occur sequentially or simultaneously: (1) transfer of electrons from In_2O_3 to ZnO due to the difference in E_F between the two materials and (2) trapping of electrons by the surface states in the interfacial layer. This carrier trapping would create depletion layers in both the In_2O_3 and ZnO near the interface and an energy barrier at the In_2O_3−ZnO interface. Consequently, the actual energy band diagram of the In_2O_3−ZnO junction after equilibrium would be similar to that near the grain boundary of polycrystalline silicon (Figure 4c). The width of the surface depletion layer is known to be on the order of Debye length λ_D.[35] A depletion layer with a thickness of ∼λ_D(In_2O_3) + λ_D(ZnO) due to the In_2O_3−ZnO interface as well as that with a thickness of ∼λ_D(ZnO) due to

dx.doi.org/10.1021/am501975v | ACS Appl. Mater. Interfaces 2014, 6, 9595−9600

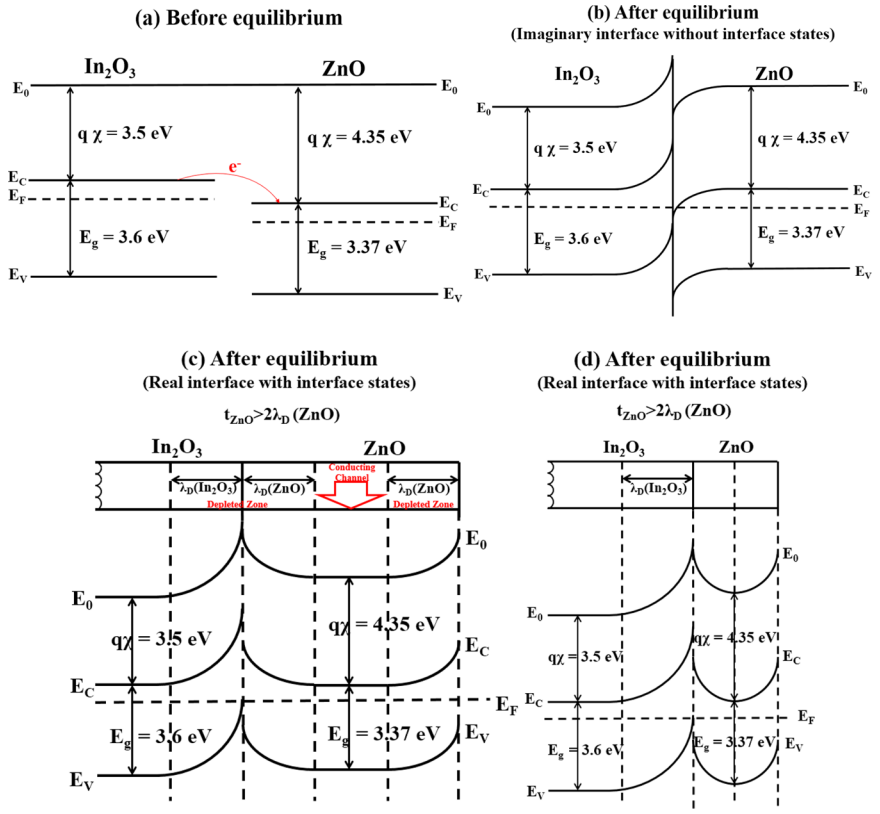

Figure 4. Energy band diagram of the In_2O_3–ZnO system (a) before and (b) after equilibrium, showing imaginary interface without interface states, (c) after equilibrium, showing real interface with interface states, $t_{ZnO} > 2\lambda_D(ZnO)$, (d) after equilibrium, showing real interface with interface states, $t_{ZnO} < 2\lambda_D(ZnO)$: (direct) energy bandgap of In_2O_3 = 3.6 eV,[31] electron affinity of In_2O_3 = 3.5 eV,[29] energy bandgap of ZnO = 3.37 eV,[32] electron affinity of ZnO = 4.35 eV,[30] $\lambda_D(In_2O_3) \approx 25$ nm,[33] and $\lambda_D(ZnO) = \sim 22$ nm.[13,15] The diagram is not drawn to scale.

the outer surface of the ZnO shell would be created in each In_2O_3-core/ZnO-shell nanowire. Upon exposure to air, oxygen molecules will extract electrons from the conduction band of ZnO so that the ZnO shell with a thickness larger than $2\lambda_D(ZnO)$ would be partly depleted of electrons. In contrast, the ZnO shell with a thickness smaller than $2\lambda_D(ZnO)$ would be completely depleted of electrons upon exposure to air, leading to a higher resistance. On the other hand, when the core–shell nanowires are exposed to a reducing gas such as ethanol, electrons will be released back to the conduction band of the shell material ZnO because of to the injection of additional electrons. As the shell layer thickness increases, the number of electrons released back to the conduction band of ZnO will increase, resulting in a decrease in resistance. If the shell layer thickness is equal to $2\lambda_D(ZnO)$, the shell layer will have a maximum number of electrons; i.e., the number of electrons released back to the conduction band of ZnO will be maximized, leading to the lowest resistance and thereby the highest sensitivity. On the other hand, if the shell layer thickness increases further than $2\lambda_D(ZnO)$, then the number of electrons released back to the conduction band will decrease so that the resistance will increase again and limited response will be obtained. In Katoch et al.'s study the depletion layer thickness λ_D due to the core–shell interface was ignored in determining the optimum shell layer thickness.

Another factor that should be considered when explaining the enhanced sensitivity of the core–shell nanowires is building of a potential barrier at the In_2O_3–ZnO interface due to electron trapping into interface states. A well known barrier-controlled carrier transport mechanism could be used to explain the enhanced sensitivity of the core–shell nanowires. The potential barrier was modulated by adsorption and desorption of gas molecules, which would increase the change in resistance. In other words, the heterojunction acts as a lever in electron transfer through which the electron transfer is facilitated or restrained, resulting in enhanced sensing performances of the core–shell nanowire sensor. In addition to the potential barrier at the In_2O_3–ZnO interface, the multiple networked core–shell nanowire sensor has two other types of potential barriers that should be overcome on their pathways by carriers before carriers reach the electrode of the sensor: the potential barrier built at the ZnO–ZnO homojunction where two nanowires intersect or contact each other and that at the ZnO grain boundary, even though the contribution of these two additional types of potential barriers might be smaller than that of the potential barrier at the In_2O_3–ZnO interface.

According to Singh et al. In_2O_3/ZnO core–shell nanowires showed stronger responses to reducing gases including CO, H_2, and ethanol than pristine In_2O_3, whereas pristine In_2O_3 nanowires showed a superior response to an oxidizing gas, NO_2.[11] Katoch at al. also concluded that core–shell nanofiber sensors are efficient only for the detection of reducing, not oxidizing, gases.[15] Their findings or statements may be partially correct. Nevertheless, it is difficult to accept their conclusion because the enhanced sensing performances of several core–shell one-dimensional (1D) nanostructures toward oxidizing gases have also been reported over the past several years. Jin et al. showed that multiple networked Ga_2O_3-core/ZnO-shell nanorod sensors had a 692-fold stronger response to 100 ppm of NO_2 at 300 °C than pristine Ga_2O_3 nanorod sensors.[13] Choi

et al. reported that the SnO_2−ZnO core−shell nanofiber sensors showed significantly improved sensing properties than the ZnO nanofiber sensors.[5] The responses of the SnO_2−ZnO core−shell nanofiber sensors to 70−2000 ppm of O_2 and to 1−5 ppm of NO_2 were in the range of 0.2−3.2 and 0.1−0.4, respectively. For comparison, they also reported that the response of ZnO nanowires to 10−50 ppm of O_2 was <0.6, that of ZnO nanorods to 100 ppb of NO_2 was 0.4, and that of SnO_2 nanobelts to 300 ppb of NO_2 was 2.3. Hwang et al. also reported that the response of ZnO−SnO_2 core−shell nanowires to 10 ppm of NO_2 was ∼33 times stronger than that of ZnO nanowires at 200 °C.[6] The enhanced responses of core−shell 1D nanostructures to oxidizing gases cannot be explained using only the surface depletion model but can be explained by a combination of the surface depletion model and the potential barrier-controlled carrier transport model.

According to the surface depletion model, the change in resistance in the core−shell nanostructures with a shell layer thickness less than $2\lambda_D$(ZnO) might be smaller than that in pristine nanostructures because no electrons are available in the shells of the core−shell nanostructures to react with the gas molecules because of complete depletion upon exposure to an oxidizing gas. On the other hand, three different potential barriers exist in the multiple networked nanowire sensor: at the core−shell interface due to the electron trapping by interface states, at the contact of two nanowires, and at the shell grain boundary. According to the potential barrier-controlled carrier transport model, the change in resistance induced by modulation of the potential barriers by adsorption and desorption of gas molecules might be large enough to overcome the smaller change in resistance due to the radial modulation of the depletion layer. In other words, the potential barrier-controlled carrier transport mechanism might be predominant over the surface depletion mechanism. Therefore, the enhanced sensing properties of the core−shell nanowires toward ethanol can be explained based on the potential barrier-controlled carrier transport model combined with the surface depletion model; the former is predominant over the latter. Because of the former of these two mechanisms, the response of core−shell 1D nanostructures to oxidizing gases could be stronger than that of pristine nanostructures even though it is inferior to the response to reducing gases.

4. CONCLUSIONS

Multiple networked In_2O_3-core/ZnO-shell nanowire sensors showed far stronger electrical response to ethanol gas at 300 °C than pristine In_2O_3 nanowire sensors. The In_2O_3/ZnO core−shell nanowires showed more than 6-fold stronger response to 1000 ppm ethanol at 300 °C than pristine In_2O_3 nanowires. The response of the core−shell nanostructures to ethanol also showed a strong dependence on the shell layer width. The strongest response to ethanol was obtained with a shell layer thickness of ∼44 nm, corresponding to the sum of the maximum widths of the depletion layers formed at the core−shell interface and shell outer surface, $2\lambda_D$(ZnO). The enhanced sensing properties of the core−shell nanowires toward ethanol can be explained based on the potential barrier-controlled carrier transport model combined with the surface depletion model; the former is predominant over the latter. Because of the former of these two mechanisms, the response of core−shell 1D nanostructures to oxidizing gases could be stronger than that of pristine nanostructures even though it is inferior to the response to reducing gases.

■ ASSOCIATED CONTENT

Supporting Information

Figure S1 showing the ZnO shell layer vs the number of ALD cycles. This material is available free of charge via the Internet at http://pubs.acs.org.

■ AUTHOR INFORMATION

Corresponding Author

*Phone: +82 32 860 7536. Fax: +82 32 862 5546. E-mail: cmlee@inha.ac.kr.

Notes

The authors declare no competing financial interest.

■ ACKNOWLEDGMENTS

This study was supported by Basic Science Research Program through the National Research Foundation of Korea (NRF) funded by the Ministry of Education (Grant 2010-0020163).

■ REFERENCES

(1) Kolmakov, A.; Zhang, Y.; Cheng, G.; Moskovits, M. Detection of CO and O_2 Using Tin Oxide Nanowire Sensors. *Adv. Mater.* **2003**, *15*, 997−1000.

(2) Liu, Y.; Koep, E.; Liu, M. A Highly Sensitive and Fast-Responding SnO_2 Sensor Fabricated by Combustion Chemical Vapor Deposition. *Chem. Mater.* **2005**, *17*, 3997−4000.

(3) Law, M.; Kind, H.; Messer, B.; Kim, F.; Yang, P. Photochemical Sensing of NO_2 with SnO_2 Nanoribbon Nanosensors at Room Temperature. *Angew. Chem., Int. Ed.* **2002**, *114*, 2511−2514.

(4) Park, J. Y.; Choi, S. W.; Lee, J. W.; Lee, C.; Kim, S. S. Synthesis and Gas Sensing Properties of TiO_2−ZnO core−shell nanofibers. *J. Am. Ceram. Soc.* **2009**, *92*, 2551−2554.

(5) Choi, S. W.; Park, J. Y.; Kim, S. S. Synthesis of SnO_2−ZnO Core−Shell Nanofibers via a Novel Two-Step Process and Their Gas Sensing Properties. *Nanotechnology* **2009**, *20*, 465603−465608.

(6) Hwang, I. S.; Kim, S. J.; Choi, J. K.; Choi, J.; Ji, H.; Kim, G. T.; Cao, G.; Lee, J. H. Synthesis and Gas Sensing Characteristics of Highly Crystalline ZnO−SnO_2 Core−Shell Nanowires. *Sens. Actuators, B* **2010**, *148*, 595−600.

(7) Chen, Y. J.; Xiao, G.; Wang, T. S.; Zhang, F.; Ma, Y.; Gao, P.; Zhu, C. L.; Zhang, E.; Xu, Z.; Li, Q. H. α-MoO_3/TiO_2 Core/Shell Nanorods: Controlled-Synthesis and Low-Temperature Gas Sensing Properties. *Sens. Actuators, B* **2011**, *155*, 270−277.

(8) Sun, P.; Sun, Y.; Ma, J.; You, L.; Lu, G.; Fu, W.; Li, M.; Yang, H. Synthesis of Novel SnO_2/$ZnSnO_3$ Core−Shell Microspheres and Their Gas Sensing Properties. *Sens. Actuators, B* **2011**, *155*, 606−611.

(9) Chen, Y. J.; Xiao, G.; Wang, T. S.; Zhang, F.; Ma, Y.; Gao, P.; Zhu, C. L.; Zhang, E.; Xu, Z.; Li, Q. H. Synthesis and Enhanced Gas Sensing Properties of Crystalline CeO_2/TiO_2 Core/Shell Nanorods. *Sens. Actuators, B* **2011**, *156*, 867−874.

(10) Jang, Y. G.; Kim, W. S.; Kim, D. H.; Hong, S. H. Fabrication of Ga_2O_3/SnO_2 Core−Shell Nanowires and Their Ethanol Gas Sensing Properties. *J. Mater. Res.* **2011**, *26*, 2322−2327.

(11) Singh, N.; Ponzoni, A.; Gupta, R. K.; Lee, P. S.; Comini, E. Synthesis of In_2O_3−ZnO Core−Shell Nanowires and Their Application in Gas Sensing. *Sens. Actuators, B* **2011**, *160*, 1346−1351.

(12) Zhang, J.; Liu, X.; Wang, L.; Yang, T.; Guo, X.; Wu, S.; Wang, S.; Zhang, S. Synthesis and Gas Sensing Properties of α-Fe_2O_3@ZnO Core−Shell Nanospindles. *Nanotechnology* **2011**, *22*, 185501−185507.

(13) Jin, C.; Park, S.; Kim, H.; Lee, C. Ultrasensitive Multiple Networked Ga_2O_3-Core/ZnO-Shell Nanorod Gas Sensors. *Sens. Actuators, B* **2012**, *161*, 223−228.

(14) Chen, I. C.; Lin, S. S.; Lin, T. J.; Hsu, C. L.; Hsueh, T. J.; Shieh, T. Y. The Assessment for Sensitivity of a NO_2 Gas Sensor with $ZnGa_2O_4$/ZnO Core−Shell Nanowires—A Novel Approach. *Sensors* **2010**, *10*, 3057−3072.

(15) Katoch, A.; Choi, S. W.; Sun, G. J.; Kim, S. S. An Approach to Detecting a Reducing Gas by Radial Modulation of Electron-Depleted Shells in Core−Shell Nanofibers. *J. Mater. Chem. A* **2013**, *1*, 13588−13596.
(16) Gurlo, A.; Barsan, N.; Weimar, U.; Ivanovskaya, M.; Taurion, A.; Siciliano, P. Polycrystalline Well-Shaped Blocks of Indium Oxide Obtained by the Sol−Gel Method and Their Gas-Sensing Properties. *Chem. Mater.* **2003**, *15*, 4377−4383.
(17) Atashbar, M. Z.; Gong, B.; Sun, H. T.; Wlodarski, W.; Lamb, R. Investigation on Ozone-Sensitive In_2O_3 Thin Films. *Thin Solid Films* **1999**, *354*, 222−226.
(18) Bianchi, S.; Comini, E.; Ferroni, M.; Faglia, G.; Vomiero, A.; Sberveglieri, G. Indium Oxide Quasi-Monodimensional Low Temperature Gas Sensor. *Sens. Actuators, B* **2006**, *118*, 204−207.
(19) Ivanonskaya, M.; Gurlo, A.; Bogdanov, P. Mechanism of O_3 and NO_2 Detection and Selectivity of In_2O_3 Sensors. *Sens. Actuators, B* **2001**, *77*, 264−267.
(20) Mccue, J. T.; Ying, J. Y. SnO_2−In_2O_3 Nanocomposites as Semiconductor Gas Sensors for CO and NOx Detection. *Chem. Mater.* **2007**, *19*, 1009−1015.
(21) Zhan, Z. L.; Jiang, D. G.; Xu, J. Q. Investigation of a New In_2O_3-Based Selective H_2 Gas Sensor with Low Power Consumption. *Mater. Chem. Phys.* **2005**, *90*, 250−254.
(22) Chu, X. F.; Wang, C. H.; Jiang, D. L.; Zheng, C. M. Ethanol Sensor Based on Indium Oxide Nanowires Prepared by Carbothermal Reduction Reaction. *Chem. Phys. Lett.* **2004**, *399*, 461−464.
(23) Xu, J.; Chen, Y.; Shen, J. Ethanol Sensor Based on Hexagonal Indium Oxide Nanorods Prepared by Solvothermal Methods. *Mater. Lett.* **2008**, *62*, 1363−1365.
(24) Arafat, M. M.; Dinan, B.; Akbar, A. S.; Haseeb, M. A. Gas Sensors Based on One Dimensional Nanostructured Metal-Oxides: A Review. *Sensors* **2012**, *12*, 7207−7258.
(25) Feng, P.; Wan, Q.; Wang, T. H. Contact-Controlled Sensing Properties of Flowerlike ZnO Nanostructures. *Appl. Phys. Lett.* **2005**, *87*, 213111−213113.
(26) Safonova, O. V.; Delabouglise, G.; Chenevier, B.; Gaskov, A. M.; Labeau, M. CO and NO_2 Gas Sensitivity of Nanocrytalline Tin Dioxide Thin Films Doped with Pd, Ru and Rh. *Mater. Sci. Eng. C* **2002**, *21*, 105−111.
(27) Kolmakov, A.; Moskovits, M. Chemical Sensing and Catalysis by One-Dimensional Metal-Oxide Nanostructures. *Annu. Rev. Mater. Res.* **2004**, *34*, 151−180.
(28) Li, J.; Fan, H.; Jia, X.; Yang, W.; Fang, P. Enhanced Blue-Green Emission and Ethanol Sensing of Co-Doped ZnO Nanocrystals Prepared by a Solvothermal Route. *Appl. Phys. A* **2010**, *98*, 537−542.
(29) Jia, H.; Zhang, Y.; Chen, X.; Shu, J.; Luo, X.; Zhang, Z.; Yu, D. Efficient Field Emission from Single Crystalline Indium Oxide Pyramids. *Appl. Phys. Lett.* **2003**, *82*, 4146−4148.
(30) Alivov, Ya. I.; Kalinina, E. V.; Cherenkov, A. E.; Look, D. C.; Ataev, B. M.; Omaev, A. K.; Chukichev, M. V.; Bagnall, D. M. Fabrication and Characterization of n-ZnO/p-AlGaN Heterojunction Light-Emitting Diodes on 6H-SiC Substrates. *Appl. Phys. Lett.* **2003**, *83*, 4719−4721.
(31) Kar, S.; Chakrabarti, S.; Chaudhuri, S. Morphology Dependent Field Emission from In_2O_3 Nanostructures. *Nanotechnology* **2006**, *17*, 3058−3062.
(32) Weast, R. C. *CRC Handbook of Chemistry and Physics*, 65th ed; CRC Press: Boca Raton, FL, 1984.
(33) Kim, S.; Carpenter, P. D.; Jean, R. K.; Chen, H.; Zhou, C.; Ju, S.; Janes, D. B. Role of Self-Assembled Monolayer Passivation in Electrical Transport Properties and Flicker Noise of Nanowire Transistors. *ACS Nano* **2012**, *6*, 7352−7361.
(34) Sauberlich, F.; Klein, A. Band Alignment at Oxide Semiconductor Interfaces. *Mater. Res. Soc. Symp. Proc.* **2003**, *763*, 1−6.
(35) Barsan, N.; Weimar, U. Conduction Model of Metal Oxide Gas Sensors. *J. Electroceram.* **2001**, *79*, 143−167.